Article

Nanoindentation Dynamic Mechanical Analysis of *Pinus radiata* D. Don Cell Wall Layers

Oswaldo Erazo[1], Joseph E. Jakes[2], Nayomi Plaza[2], Judith Vergara-Figueroa[1], Paulina Valenzuela[1] and William Gacitúa[1*]

[1]Department of Wood Engineering, Center for Biomaterials and Nanotechnology, Faculty of Engineering Universidad del Bío Bío, Concepción 4030000, Chile.

[2]Forest Biopolymers Science and Engineering, USDA Forest Service, Forest Products Laboratory, One Gifford Pinchot Drive, Madison, WI 53726, USA

*Correspondence: wgacitua@ubiobio.cl

Abstract: Quasistatic nanoindentation is a proven tool that provides information on the micromechanical behavior of wood cell walls. However, quasistatic tests cannot probe the time-dependent mechanical behavior shown by wood. Nanoindentation dynamic mechanical analysis (nanoDMA) can mesaure the viscoelastic properties of wood cell walls. This research aimed to study the quasistatic and viscoelastic properties of individual radiata pine wood (*Pinus radiata* D. Don) cell wall layers. To minimize variability and retrieve both properties at the same locations, a load function composed of a multiload-quasistatic function followed by dynamic reference frequency segments was developed. Nanoindentations were then performed on the S2 layer and compound corner middle lamella (CCML) of unembedded latewood cells. Because the S2 layer is anisotropic, both transverse and longitudinal-tangential wood planes were studied. In the transverse plane, the average results of the quasistatic elastic moduli (E_s) for the S2 layer and CCML were 15.7 GPa and 4.6 GPa, respectively. In the longitudinal-tangential plane, the E_s was 3.9 GPa. In the transverse section, the hardness (H) of the S2 layer and CCML were 331 MPa and 277 MPa, respectively, and in the longitudinal-tangential section H was 244 MPa. To acquire the viscoelastic properties, measurements were made over more than three decades of frequency. An increase of the storage modulus (E'), and a reduction of the loss modulus (E'') and loss factor ($\tan\delta$) as frequency increased were found in both wood orientations. The quasi-static and dynamic indentations equivalent at 0.1 Hz showed similar values for E_s and E'. This study contributes to our knowledge of wood cell wall micromechanical properties.

Keywords: Radiata pine; nanoDMA; nanomechanical properties; viscoelastic properties

1. Introduction

Wood is a versatile, environmentally friendly material with remarkable mechanical properties that make it a sustainable alternative to other materials such as plastic, steel, and concrete. Its advantageous properties stem from wood's complex multiscale structure and chemical composition. The wood cell wall is made up of polymeric components, primarily cellulose, hemicelluloses, and lignin. Each polymer has different chemical and physical properties, and they form an intricate network with one another providing strength to wood [1,2]. These wood components exhibit certain mechanical and viscoelastic behavior depending on the conditions they are exposed to, such as temperature, humidity, load type, and time [3–6]. Bulk wood mechanical properties have been evaluated under various laboratory tests [7,8]. At the micrometer scale, the mechanical properties have been studied using novel characterization techniques and state-of-the-art technologies. Studying the mechanical behavior of wood at the nanometer scale can help us understand the molecular-scale processes responsible for the phenomena we observe at the macroscopic level [9].

Nanoindentation has proven to be a useful tool to evaluate the micrometer-scale mechanical properties of the S2 layer and compound corner middle lamella (CCML) of the cell walls of different

Preprints (www.preprints.org) | NOT PEER-REVIEWED | Posted: 21 April 2023 doi:10.20944/preprints202304.0708.v1

wood species [10–15]. In a typical nanoindentation test, a carefully shaped probe is pressed into a sample following a prescribed loading protocol, which typically consists of a loading segment, a hold at maximum load segment, and an unloading segment, while both applied load and displacement are continuously measured [16]. The test can be quasistatic or dynamic. In the quasistatic test, the elastic modulus of a material is obtained from the contact area and initial slope of the unloading segment in a load vs. displacement ($P-h$) graph , whereas the hardness is calculated from the maximum load and contact area [17]. The calculations assume that during the unloading segment the material has a purely elastic behavior [18].

However, wood cell walls are polymeric materials, and thus, exhibit time-dependent elastic and plastic mechanical behavior. Therefore, elastic modulus and hardness measurements made using quasistatic nanoindentations are unique values that correspond to the chosen time-scales of the loading, hold at maximum load, and unloading segments in the load function [19,20]. Capturing time-dependent mechanical properties using quasistatic nanoindentation requires series of nanoindentations while systematically varying times for the different segments in each load function [19,20]. It is also not straightforward to calculate mechanical damping using quasistatic nanoindentation. Therefore, quasistatic nanoindentation has limitations in describing the full magnitude of the mechanical response of a viscoelastic material during the indentation process [21].

Nanoscale Dynamic Mechanical Analysis (nanoDMA) is complementary to quasistatic nanoindentation testing. The nanoDMA technique involves a small sinusoidal load superimposed on the quasistatic nanoindentation loading. By measuring the corresponding displacement amplitude and time lag between the displacement and load measurements, dynamic properties are obtained: storage modulus and loss modulus, which each represent two different components of the material's behavior [18]. The specimens are subjected to the application and release of stresses for a given time. Being a cyclic experiment, different orders of magnitude of frequencies ranging from millihertz to hundreds of Hertz can be used. The storage modulus E' is related to the stiffness or the sample's in-phase response to the applied force. Therefore, it is related to the elastic recovery of the material, which represents the amount of energy stored after an oscillation loading cycle. The loss modulus (E''), also called viscous modulus, is a parameter related to the viscous energy dissipation of a material due to the internal movement of polymeric chains [22]. The viscous state, or mechanical damping, of the material is obtained by the ratio of these two parameters and is known as the loss tangent ($\tan\delta$), which is zero for an ideal elastic material and extends to infinity for an ideal liquid [23].

The nanoDMA technique has been used to quantify mechanical changes in various materials [21,24]. This trend continues with the incorporation of additional materials with broad potential for different applications [25–28]. The viscoelastic properties of *Carapa procera* wood cell walls have been studied using various nanoindentation tests, including nanoDMA in a frequency range of 10 to 240 Hz. The reduced storage modulus and $\tan\delta$ s measured at 50 locations ranged from 7 to 15 GPa and 0.01-0.04, respectively [29]. Nano-DMA has also been used to investigate the effects of accelerated aging on the cell wall micromechanics of loblolly pine wood (*Pinus taeda*) [30]. Moreover, the modulus mapping method has been used to obtain the storage modulus in Norway spruce wood [31,32]. Similarly, using the dynamic mapping technique, micromechanical variations in phenol formaldehyde-impregnated *Pinus massoniana* samples [33] and individual phases within sapwood tissues of *Larix gmelinii* [34] have been analyzed. Dynamic nanoindentation has also been used to study the correlations of heat-treated bamboo cells and heat treatment conditions [35]. In addition to a more thorough characterization of time-dependent mechanical properties, viscoelastic characterization over wide ranges of frequency can also provide insights into microphysical processes causally linked to material properties [36]. Jakes used nanoDMA to measure the moisture-dependent $\tan\delta$ in latewood loblolly pine wood cell walls across more than three decades of frequency [37]. The results revealed a peak in $\tan\delta$ at high moisture content, which was used to causally link polymer segmental motions to intra-cell wall mineral ion diffusion. These nanoDMA results led to the discovery that mineral ion diffusion though a wood cell wall is a solid polymer diffusion process.

Preprints (www.preprints.org) | NOT PEER-REVIEWED | Posted: 21 April 2023 doi:10.20944/preprints202304.0708.v1

Nanoindentation and nanoDMA have proven to be very useful tools for studying mechanical properties in wood cell walls. However, the high variability in the mechanical properties among different wood species makes it difficult to make accurate predictions about the mechanical behavior of one species based on the data from another. In Chile, radiata pine wood accounts for 60% of the 3.11 million hectares of forest plantations [38], therefore it is the main species used there for structural applications. Thus, it is important to study the mechanical behavior at the microscale, which will contribute to have a complete picture for the design of timber structures that will be exposed to different service conditions. Yet, to the best of our knowledge there are no reports of nanoDMA for this species. Furthermore, the anisotropic E' over greater than three decades of frequency have never been reported for wood cell wall layers. The objective of this research was to study the viscoelastic properties over a frequency range of 0.1 to 200 Hz of radiata pine compound corner middle lamella (CCML) and S2 layer. The S2 layer was measured in both the transverse and longitudinal orientations. Quasistatic elastic modulus and hardness measurements were also made on the same cell wall layers. The obtained results allowed a comparison of quasistatic nanoindentation and nanoDMA measurements on the same locations in wood cell wall layers.

2. Materials and Methods

2.1. Sample origin and preparation

Samples were obtained from a strip of a radiata pine tree (*Pinus radiata* D. Don) from a 26-year-old plantation located in Los Ángeles, Bío-Bío Province, VIII region, Chile. The strip was dried to 12% moisture content in an industrial dryer. The basic bulk wood density of 0.39 $g\ cm^{-3}$ was determined according to the ASTM D2395-14 standard [39]. Small latewood blocks of 5 mm in length and a cross-sectional area of 4 x 4 mm were cut with a fine tooth saw and bonded to a steel disc with using 5-minute epoxy such that either a transverse or a tangential-longitudinal plane was facing up. Samples were not embedded in low viscosity resin to avoid possible unwanted chemical modifications by the resin [40,41]. Nanoindentation surface preparation in the unembedded wood followed the protocols described in Jakes and Stone [15]. Briefly, the specimens were fit into a Leica (Wetzlar, Germany) EM UC7 ultramicrotome equipped with a Micro Star (Huntsville, Texas) 45° diamond knife. A hand razor was used to trim a pyramid with an apex in the region of interest. To obtain smooth block face surfaces for nanoindentations, sections were cut from the apex using the diamond knife with the final sections only 100 nm thick.

2.2. Nanoindentation

Nanoindentation was performed using a Bruker-Hysitron (Minneapolis, Minnesota, USA) TriboIndenter equipped with a diamond Berkovich probe and upgraded with the nanoDMA III package. The relative humidity (RH) inside of the enclosure was maintained at 60% ± 1% RH using an InstruQuest (Coconut Creek, Florida) HumiSys HF RH generator. The temperature was not controlled but measured to be maintained between 20° ± 1°C. The calibration of the RH and temperature sensor was verified using a Control Company (Webster, TX, USA) 4085 Traceable® Hygrometer Thermometer Dew Point Meter. The machine compliance, probe area function, and tip roundness effects were determined using the procedures in [42,43] and a series of 80 nanoindentations in a fused silica calibration standard. Following the calibration reporting procedure prescribed in [42]: values for the square root of the Joslin-Oliver parameter of 1.254 ± 0.002 μm/N½, elastic modulus of 72.0 ± 0.2 GPa, and Meyer's hardness of 9.72 ± 0.03 GPa were obtained for nanoindentations with contact depths between 30 and 186 nm. No systematic variations of machine compliance or Joslin-Oliver parameter were observed in the systematic SYS plot analysis over this range of contact depths. Uncertainties in calibration measurements correspond to standard errors.

For nanoindentation, an open-loop, two-part load function was created consisting of a quasistatic multiload segment followed by a dynamic reference frequency segment (Figure 1). This load function design facilitated both quasistatic and viscoelastic micromechanical measurements from the same nanoindentation locations. A pre-nanoindentation 25 nm lift-off, 2 μm stage offset,

Preprints (www.preprints.org) | NOT PEER-REVIEWED | Posted: 21 April 2023 doi:10.20944/preprints202304.0708.v1

and reapproach was used to accurately detect the undeformed specimen surface. The multiload part was based on the multiload load function described in detail in [15]. It was designed to provide data needed for employing the structural compliance method and to measure depth-dependent elastic modulus and hardness. It consisted of eight cycles with each cycle containing four segments: (1) an effectively 2 s loading segment, (2) a 5 s hold at the cycle maximum load, (3) a 1.4 s unloading segment to 30% of the cycle maximum load, and (4) a 1 s hold at 30% of the cycle maximum load before starting the next cycle. The quasistatic multiload part ended with a loading segment after the eighth cycle that loaded to the overall nanoindentation maximum load. The multiload cycle maximum loads ranged from 4 to 81% of the overall nanoindentation maximum load. The dynamic reference frequency part was designed to assess viscoelastic properties, including storage modulus (E'), loss modulus (E''), and mechanical damping ($\tan\delta$), from 0.1 to 200 Hz. Assessing properties over such a large frequency range required about 30 minutes. Reference frequency load functions are advantageous for long duration experiments because the reference frequency segments are used to determine contact areas instead of depth [44,45]. The depth measurements become unreliable during long nanoindentation experiments because of displacement drift uncertainties. The dynamic part began with a 17 s segment at 220 Hz, then an initial 10 s reference frequency segment at 220 Hz. The remaining dynamic part consisted of a series of alternating testing frequency and 10 s reference frequency segments, before ending with a 5 s unload. There were 11 testing frequencies, which were evenly positioned on a logarithmic scale from 200 to 0.1 Hz [37].

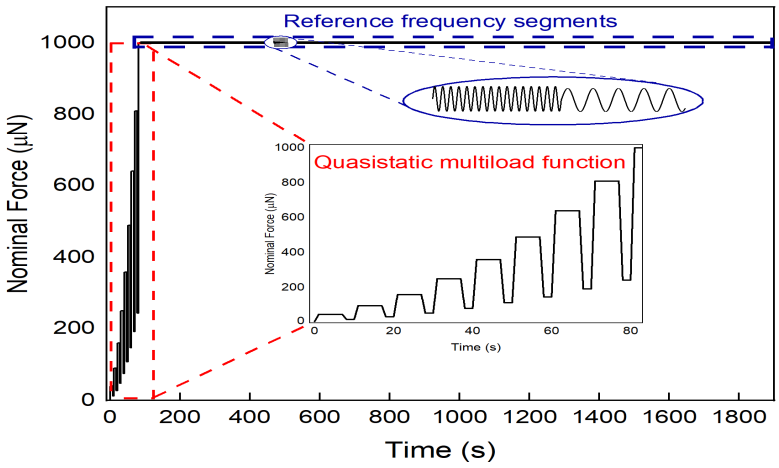

Figure 1. Load function comprises of a multiload function and a reference frequency segment.

Nanoindentation experiments followed the best practices described in [15] to minimize errors arising from misplaced nanoindentations, surface detection errors, dirty probes, displacement drift, and nanoindenter calibration or performance issues as well as structural compliances caused by nearby free edges and cellular flexing. In brief, wood specimens were placed inside of the nanoindenter enclosure and left to equilibrate 48 hours before testing. Areas for nanoindentation were chosen using the optical microscope in the TriboIndenter. Scanning probe microscopy images obtained using the nanoindentation probe were used to both place the nanoindentations in the cell wall layer of interest and to verify their placement after experiments (Figure 2). Any nanoindentation overlapping an interface was discarded. In the multiload part, unloading segments with contact depths lower than 30 nm were excluded from further analysis because tip roundness effects were detected in the fused silica calibrations below that depth. The structural compliance method [41,46] was employed using the quasistatic multiload part of the experiment to remove potential artifacts arising from nearby edges and specimen-scale flexing. Both the quasistatic and dynamic parts were corrected using the structural compliance measurement from the analysis of the multiload segments.

Preprints (www.preprints.org) | NOT PEER-REVIEWED | Posted: 21 April 2023 doi:10.20944/preprints202304.0708.v1

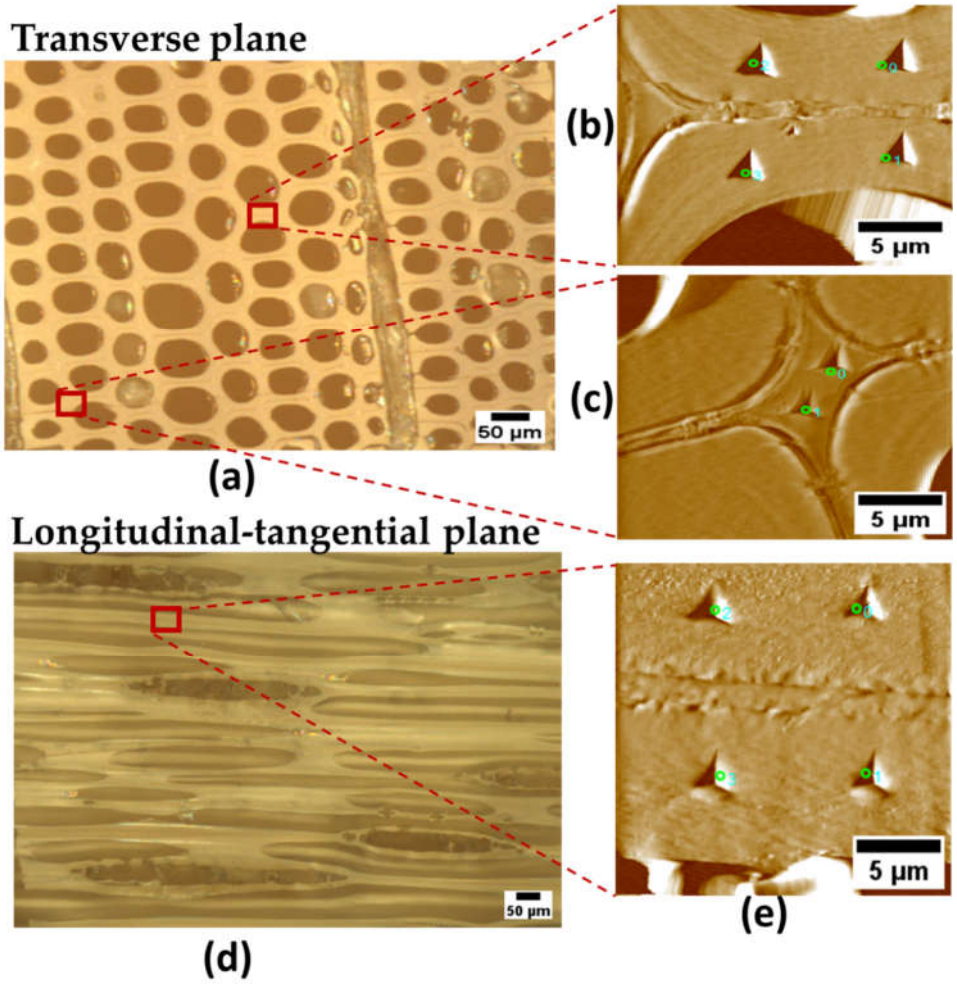

Figure 2. Cutting planes in radiata pine wood. (**a**) Transverse plane with nanoindentations on (**b**) S2 layer and (**c**) CCML, (**d**) Longitudinal-tangential plane with nanoindentations on (**e**) S2 layer.

The quasistatic reduced elastic modulus (E_r) and hardness (H) of the cell wall layers were then calculated using the following equations:

$$E_r = \frac{S\sqrt{\pi}}{2\sqrt{A_c}} \quad (1)$$

$$H = \frac{P_{max}}{A_c} \quad (2)$$

where S is the contact stiffness of the unloading segment, A_c is the projected contact area, and P_{max} is the maximum load immediately prior to unloading. To evaluate the specimen elastic modulus of the sample (E_s), while considering the probe contributions to the E_r, the following equation was used:

$$\frac{1}{E_r} = \left(\frac{1-\nu_s^2}{E_s} + \frac{1-\nu_d^2}{E_d}\right) \quad (3)$$

where E_d is the elastic modulus of the diamond probe (1137 GPa), ν_d and ν_s are the Poisson's ratio of diamond probe and sample, respectively. For this work, $\nu_d = 0.07$ and $\nu_s = 0.3$ were used [47].

Preprints (www.preprints.org) | NOT PEER-REVIEWED | Posted: 21 April 2023 doi:10.20944/preprints202304.0708.v1

The storage modulus (E'), loss modulus (E''), and the mechanical damping ($\tan\delta$) were obtained directly from [48]:

$$E' = \frac{(1-\nu_s^2)K_s\sqrt{\pi}}{2\sqrt{A_c^{ref}}} \quad (4)$$

$$E'' = \frac{(1-\nu_s^2)\omega C_s\sqrt{\pi}}{2\sqrt{A_c^{ref}}} \quad (5)$$

$$\tan\delta = \frac{E''}{E'} \quad (6)$$

K_s and C_s are the dynamic stiffness and damping coefficients, respectively, ω is the radial frequency, ν_s is the Poisson's ratio of the sample, $\nu_s = 0.3$, and A_c^{ref} is the reference contact area calculated using

$$A_c^{ref} = \left(\frac{(1-\nu_s^2)K_s\sqrt{\pi}}{2E'_{ref}}\right)^2 \quad (7)$$

where E'_{ref} is the E' calculated from the initial reference frequency segment. For each testing frequency segment, A_c^{ref} was calculated using the K_s from the reference frequency segment immediately following the testing segment.

3. Results and Discussion

3.1. Quasistatic nanoindentations

In this investigation, unembedded specimens were used. Therefore, nanoindentations in wood cell walls layers were always nearby heterophase interfaces, such as the free edge of a lumen surface, and the entire open cellular structure could flex under loading. Thus, for each nanoindentation, structural compliance method was employed using the initial quasistatic multiload segments. This allowed to reduce or eliminate the effects associated with the heterophase interfaces and specimen-scale flexing, which if left unaccounted for can lead to an overestimation or underestimation of hardness and elastic modulus [15]. Because the structural compliance correction is location dependent, the structural compliance correction calculated from the quasistatic multiload portion was applied to the entire nanoindentation experiment, including the dynamic portions. Therefore, both the quasistatic multiload and dynamic viscoelastic experiments were corrected for structural compliances.

Figure 3 shows the behavior of the elastic modulus and hardness in the multiload segments as a function of the contact depth of each of the indentations performed. It is observed that the results lower than 30 nm were discarded because tip roundness effects. It is clear that the hardness and elastic modulus values for samples are almost constant throughout the indentation depth. The scatter in each nanonidentation results to a good part from the variability of the S2 layer and CCML of the samples. Although variability is present in all the quasistatic results, no systematic trends in mechanical behavior with contact depth could be observed. In relation to the elastic modulus in the transverse orientation, an average of 15.7 ± 1.9 GPa was obtained, with a coefficient of variation of 12.5% (Figure 3a). This variation is generated by the orientation of the microfibril angles [49], which is the dominant parameter of microstructural influence on wood stiffness. The degree of inclination of the microfibril angle can be affected by the proximity to the cell lumen and pits [12]. The elastic

Preprints (www.preprints.org) | NOT PEER-REVIEWED | Posted: 21 April 2023 doi:10.20944/preprints202304.0708.v1

modulus values found in this research are slightly higher than those reported by [50] and [51]. On the other hand, the hardness presented an average of 331.1 ± 26.3 MPa (Figure 3b). The variation in the hardness measurements was 7.9%. This result is slightly lower than that reported by Moon (2009) in non-impregnated radiata pine latewood cells [52], but is within the range of hardness reported for another pine species [14]. This discrepancy in results in both elastic modulus and hardness could be due to variability in wood structure and more specifically microfibril angles, which can even vary between different growth rings, resin embedment, or differences in the RH of the testing environment.

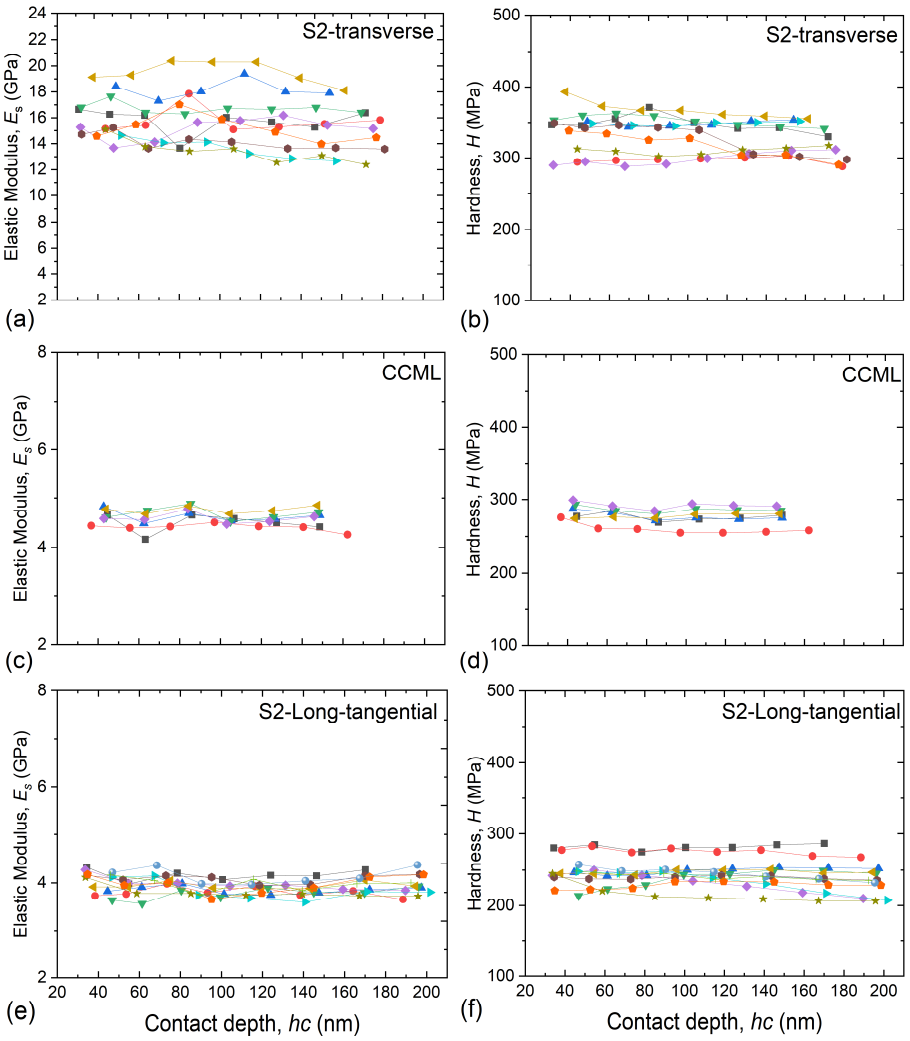

Figure 3. Elastic modulus and hardness of wood cell walls obtained from individual nanoindentations. (**a-b**) S2 layer in the transverse orientation; (**c-d**) CCML in the transverse orientation; **(e-f)** S2 layer in the longitudinal-tangential orientation. Each colored curve represents the complete multiload segment of a nanoindentation.

The average value of the elastic modulus of the CCML was 4.6 ± 0.2 GPa and a coefficient of variation of 3.6%. The value of the elastic modulus is clearly reduced in the middle lamella, which is approximately 30% of the result found in the S2 layer (Figure 3c). These differences between the mechanical properties of the secondary wall and the middle lamella are due to the proportion of structural components [53]. Concerning the hardness of the CCML, an average of 277.6 ± 11.4 MPa and a coefficient of variation of 4.1% were found (Figure 3d). This low variability is justified by the fact that the middle lamella is mainly constituted by lignin around 86% [54], while in the S2 layer, apart from cellulose, there is also the presence of lignin and hemicelluloses. Likewise, the higher coefficient of variation of the hardness in the S2 layer is due to the spatial variation in the distribution

 doi:10.20944/preprints202304.0708.v1

of lignin in the cell wall [55]. Some authors have found no difference between the hardness of the S2 layer and the middle lamella [12,53]. However, the results here showed a contrast, since the hardness values in the CCML are approximately 16% lower. This may be due to a higher lignin concentration contributing in two ways, indirectly increasing packing density of the cell wall by filling the space between hemicellulose and cellulose fibrils and directly to the higher cell wall hardness [55]. The difference could also be caused by resin embedment in previous experiments or differences in the RH of the testing environment.

The quantitative analysis of the indentations performed on the S2 layer in the longitudinal-tangential plane revealed average values of the elastic transverse modulus of 3.9 ± 0.2 GPa, with a coefficient of variation of 4.4% (Figure 3e), while the hardness presented average values of 243.9 ± 19.8 MPa and a coefficient of variation of 8.9% (Figure 3f). The average value of the elastic modulus is 4 times lower than the longitudinal elastic modulus. Similarly, [56] found in the S2 layer of spruce wood up to 5.8 times higher values in the longitudinal elastic modulus than the transversal elastic modulus. This is because the direction of application of the indenter probe is perpendicular to the arrangement of the cellulose fibrils in the S2 layer. Thus, when performing an indentation in this orientation, the fibrils are in mechanical series with the more compliant amorphous polymers in the matrix, which therefore have the greatest influence on the transverse elastic modulus [1].

3.2. NanoDMA

When wood is put into service it can be subjected to different time scales of stresses and the mechanical behavior of material varies as a function of frequency. Thus, depending on the application of the oscillatory loads, it will exhibit different properties. The viscoelastic response of wood is a result of the structure and relaxations of the structural wood polymer components and their interactions with environmental conditions (humidity and temperature). This leads to a complex deformation mechanism in response to stress. Figure 4 shows the viscoelastic properties of radiata pine wood S2 layer in the transverse direction. The influence of temperature on storage modulus has been extensively studied. It has been found that the modulus decreases with increasing temperature [57]. However, this behavior is opposite to the frequency, that is, the storage modulus increases as the frequency increases, obtaining lower values of 14.3 and 14.7 GPa for frequencies lower than 1 Hz and the maximum value (16.9 GPa) was found at higher frequencies. However, it is observed that at the frequency of 93.5 Hz, the value of the storage modulus is similar to that at the frequency of 200 Hz. This value is higher than that reported by [32] on Norway Spruce wood cell wall. These researchers obtained an average storage modulus of 15.5 GPa and 12.4 GPa for air-dried and artificially dried wood, respectively, using modulus mapping at a frequency of 80 Hz. The increase of storage modulus with frequency was also observed in the *Carapa* species cell wall using nanoDMA in a frequency range of 10 to 240 Hz [29] and in Chinese fir wood [58].

Preprints (www.preprints.org) | NOT PEER-REVIEWED | Posted: 21 April 2023 doi:10.20944/preprints202304.0708.v1

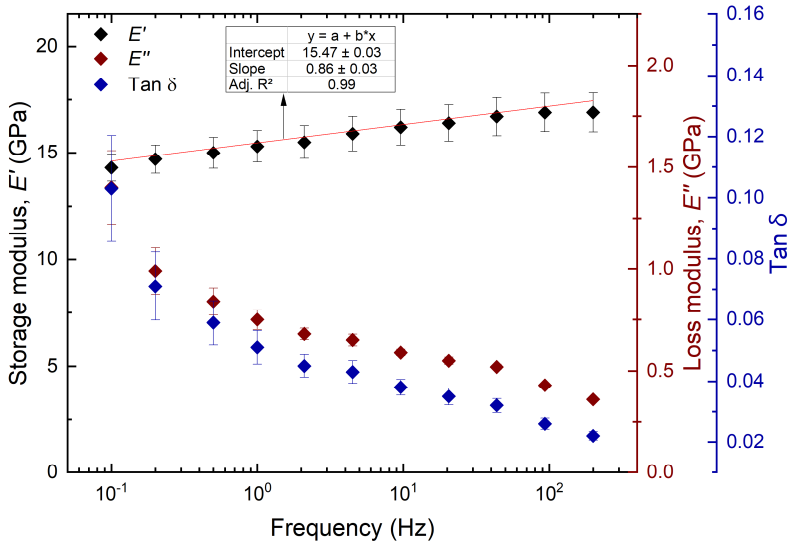

Figure 4. Viscoelastic properties of the S2 cell wall layer in the transverse plane. Error bars are the standard error.

As seen in Figure 4, the increase in modulus is linear and fits the logarithmic scale of the frequency with an adjusted coefficient of determination (R^2) of 0.99. The reason for this increase in storage modulus is due to the shorter exposure times (cycle/s) of the material to the load. Therefore, the polymer chains will be able to recover faster, and the amount of stored energy is higher. The polymer chains have minimal movements, and this makes it behave as a rigid material. In contrast to the storage modulus, it is observed that the amount of dissipated energy or loss modulus increases as the frequency decreases, with values from 1.40 GPa for the lowest frequency to 0.36 GPa at 200 Hz. Therefore, it is evident that the material has a stiffer behavior at high frequencies because the viscous response is related to the relaxation time of the material. At high frequencies, the duration of each cycle time is shorter, therefore, there is less time for the chains to relax, begin to move and reach new conformations in response to the applied stress. Consequently, the viscous response of the material is lost [59]. On the other hand, when wood is subjected to cyclic loading, it loses energy during the deformation process. This loss factor is smaller as the frequency becomes larger, since there is less energy dissipated due to the small molecular movement. Here, the tan δ decreased from 0.10 at the lowest frequency to 0.02 at 200 Hz. A decrease in tan δ was also observed by [29,37].

Similarly, for the CCML (Figure 5), the values of the storage modulus increased as the frequency increased. A linear correlation was obtained with an $R^2 = 0.99$. Compared to the S2 layer, the storage modulus values are considerably lower. At the maximum frequency, 200 Hz, the storage modulus was 5.7 GPa. This value decreased until it reached 4.4 GPa at the frequency of 0.1 Hz. Likewise, as indicated in the quasistatic indentations section, the decrease in modulus is related to the chemical composition of the CCML, which is mostly constituted by lignin with some hemicelluloses and lacks the highly organized stiff cellulose fibrils. On the other hand, following the same order of the frequency described above, the loss modulus presented values of 0.22 GPa and 0.39 GPa, respectively. Evidently, the loss modulus decreased as the frequency increased. However, unlike the S2 layer this was not a featureless decrease in the loss modulus with increasing frequency. There is a decrease in the loss modulus from 0.1 to 0.5 Hz, followed by an increase until 4.5 Hz, and another a decrease in the loss modulus until reaching the maximum frequency. The variation of the tan δ as a function of frequency is also shown. The plateau in tan δ here is very similar to that previously observed in the loblolly pine CCML [37]. Jakes [37] also tested under higher RH conditions and observed that the plateau in Figure 5 is actually a peak in tan δ that clearly emerges at higher frequencies under higher RH conditions.

Preprints (www.preprints.org) | NOT PEER-REVIEWED | Posted: 21 April 2023 doi:10.20944/preprints202304.0708.v1

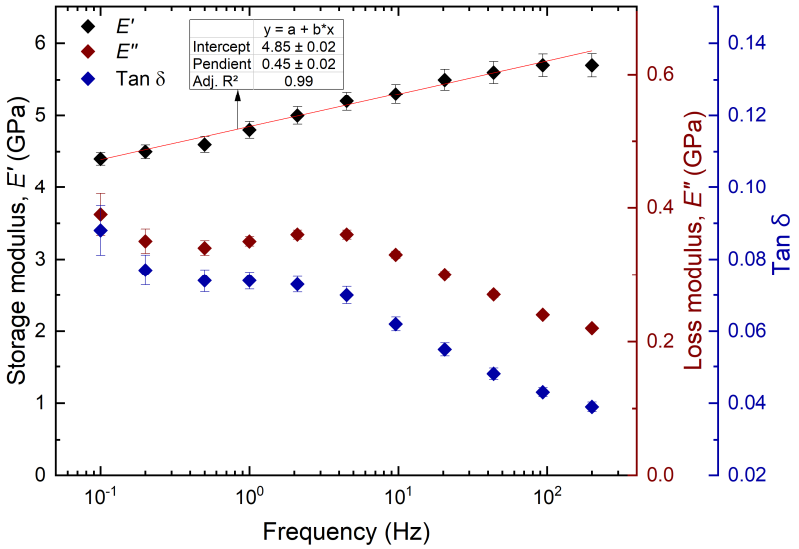

Figure 5. Viscoelastic properties of the CCML in the transverse plane. Error bars are the standard error.

Figure 6 shows the viscoelastic properties for the S2 layer in the longitudinal-tangential orientation. The storage modulus in this direction increased with frequency. A strong linear correlation R^2= 0.99 is shown. It is observed that the storage modulus at the maximum frequency (200 Hz) is slightly lower than the value reported for the CCML and up to 3 times lower than the elastic modulus of the S2 layer in the transverse direction. This trend is maintained for the remaining frequencies. The loss modulus increases with increasing frequency until it reaches a peak at frequency 4.5 Hz, then decreases with increasing frequency. The tan δ changes with frequency, it tends to decrease towards higher frequencies. However, it is observed that there is a plateau. Again, this plateau in tan δ here is very similar to that previously observed in the loblolly pine S2 layer tested in a longitudinal plane, which was attributed to a tan δ peak that emerges at higher frequencies under higher RH conditions [37]. In general, the CCML and the S2 layer tested in the longitudinal-tangential plane behave similarly, despite the marked differences in the proportions of their underlying structural components. However, during testing on the longitudinal plane, the stress is applied in the direction perpendicular to the long, stiff axis of the cellulose fibrils in the S2 layer. Thus, the fibrils are in mechanical series with the more compliant amorphous polymers in the matrix, which therefore have the greatest influence on the transverse elastic modulus. The similarity between the transverse S2 layer and CCML viscoelastic properties is likely because the mechanical responses are both being similarly dominated by the matrix polymers lignin and hemicelluloses.

Preprints (www.preprints.org) | NOT PEER-REVIEWED | Posted: 21 April 2023 doi:10.20944/preprints202304.0708.v1

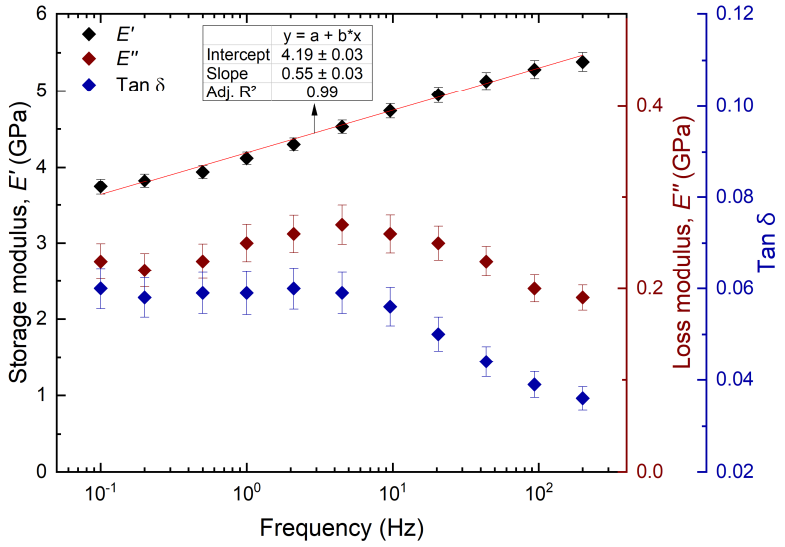

Figure 6. Viscoelastic properties of the S2 layer in the longitudinal-tangential plane. Error bars are the standard error.

The load function used made it possible to obtain both quasistatic and dynamic properties at the same nanoindentation locations. For comparison, a frequency is estimated for the quasistatic experiments using the transformation $f = 1/2\pi t_{ul}$ where t_{ul} is the 2 s unloading time [19,36]. Therefore, the approximate frequency corresponding to the quasistatic results is about 0.08 Hz. When comparing the values obtained for quasi-static and dynamic indentations equivalent at a frequency of 0.1 Hz, it is found that the elastic and storage moduli are relatively similar. When there is no damping, the elastic modulus is similar to the storage modulus [60]. However, when it comes to wood, this does not occur markedly due to its viscoelastic nature, which was evident in the results shown. Table 1 shows the results of the elastic and dynamic moduli for the S2 layer and CCML.

Table 1. Elastic and storage moduli for the S2 layer and CCML in the different wood planes

	Elastic modulus **(GPa)**	***Storage modulus*** **(GPa)**
S2-transverse plane	15.7 (1.9)	14.3 (0.62)
CCML-transverse plane	4.6 (0.2)	4.4 (0.08)
S2 longitudinal-tangential plane	3.9 (0.2)	3.7 (0.10)

Values in parenthesis are the standard error.

4. Conclusions

The application of a load function composed of a multiload segment and a reference frequency segment provided results for the quasistatic and dynamic mechanical properties of the S2 layer and CCML of radiata pine wood. It is important to note that several nanoindentations were performed in different cell walls, but for each nanoindentation both types of properties were obtained, which allows having thorough data on the mechanical behavior of the wood cell walls that can be used for both engineering applications as well as investigating causal links between microphysical processes and material properties. The small variations in the nanoindentations performed reflected the inhomogeneities of the wood structure. The mechanical properties of wood are a function of the chemical composition and the arrangement of the polymeric chains. The chemical nature of each structural component gives the wood a viscoelastic behavior, which is dependent on the service conditions of the wood. When subjected to cyclic loading, the material will respond according to the intensity of the stress. In this investigation, for the S2 layer and CCML, the storage modulus increased

with frequency, while the viscous response of the material remained relatively constant or decreased. When comparing the values of the elastic and storage moduli obtained at a frequency of 0.1 Hz, it is observed that they are very similar, other than for the elastic modulus of the S2 layer in the transverse orientation, whose value is relatively higher than the storage modulus. Radiata pine is a species that has a high projection for structural use. This study contributes to generate information on microscale properties, which can be used in the development and design of structural works.

Author Contributions: Conceptualization, O.E. and J.E.J.; methodology, J.E.J.; validation, J.E.J., O.E. and W.G.; formal analysis, O.E.; J.E.J. and N.P.; investigation, O.E., J.E.J. and W.G; resources, W.G.; data curation, J.E.J. and O.E.; writing—original draft preparation, O. E.; writing—review and editing, O. E.; J.E.J.; N.P.; W.G.; J.V-F.; P.V.; visualization, O.E.; J.E.J.; N.P.; W.G.; J.V-F.; P.V.; supervision, J.E.J.; project administration, W.G.; funding acquisition, W.G. All authors have read and agreed to the published version of the manuscript.

Funding: This research was funded by the National Agency for Research and Development (ANID) through the Research Project FONDECYT No. 1191228.

Data Availability Statement: Data can be available upon reasonable request to the corresponding author.

Acknowledgments: The authors would like to acknowledge to the USDA Forest Service, Forest Products Laboratory for the support of the Nanoindentation testing. Oswaldo Erazo would like to thank the University of Bío Bío for the Doctoral Scholarship and Research Grant.

Conflicts of Interest: The authors declare no conflict of interest.

References

1. Bergander, A.; Salmén, L. Cell Wall Properties and Their Effects on the Mechanical Properties of Fibers. *J. Mater. Sci.* **2002**, *37*, 151–156, doi:10.1023/A:1013115925679.
2. Winandy, J.E.; Rowell, R.M. *Chemistry of Wood Strength*; 2012; ISBN 9781439853818.
3. Kaboorani, A.; Blanchet, P.; Laghdir, A. A Rapid Method to Assess Viscoelastic and Mechanosorptive Creep in Wood. *Wood Fiber Sci.* **2013**, *45*, 370–382.
4. Fathi, H.; Kazemirad, S.; Nasir, V. A Nondestructive Guided Wave Propagation Method for the Characterization of Moisture-Dependent Viscoelastic Properties of Wood Materials. *Mater. Struct. Constr.* **2020**, *53*, 1–14, doi:10.1617/s11527-020-01578-6.
5. Sharma, M.; Brennan, M.; Chauhan, S.S.; Entwistle, K.M.; Altaner, C.M.; Harris, P.J. Wood Quality Assessment of Pinus Radiata (Radiata Pine) Saplings by Dynamic Mechanical Analysis. *Wood Sci. Technol.* **2015**, *49*, 1239–1250, doi:10.1007/s00226-015-0769-x.
6. Pearson, H.; Gabbitas, B.; Ormarsson, S. Tensile Behaviour of Radiata Pine with Different Moisture Contents at Elevated Temperatures. *Holzforschung* **2012**, *66*, 659–665, doi:10.1515/hf-2011-0185.
7. Hu, W.; Chen, B.; Zhang, T. Experimental and Numerical Studies on Mechanical Behaviors of Beech Wood under Compressive and Tensile States. *Wood Res.* **2021**, *66*, 27–38, doi:10.37763/WR.1336-4561/66.1.2738.
8. Nowak, T.; Patalas, F.; Karolak, A. Estimating Mechanical Properties of Wood in Existing Structures—Selected Aspects. *Materials (Basel).* **2021**, *14*, doi:10.3390/ma14081941.
9. Eder, M.; Arnould, O.; Dunlop, J.W.C.; Hornatowska, J.; Salmén, L. Experimental Micromechanical Characterisation of Wood Cell Walls. *Wood Sci. Technol.* **2013**, *47*, 163–182, doi:10.1007/s00226-012-0515-6.
10. Gindl, W.; Gupta, H.S.; Schöberl, T.; Lichtenegger, H.C.; Fratzl, P. Mechanical Properties of Spruce Wood Cell Walls by Nanoindentation. *Appl. Phys. A Mater. Sci. Process.* **2004**, *79*, 2069–2073, doi:10.1007/s00339-004-2864-y.
11. Gacitua, W.; Bahr, D.; Wolcott, M. Damage of the Cell Wall during Extrusion and Injection Molding of Wood Plastic Composites. *Compos. Part A Appl. Sci. Manuf.* **2010**, *41*, 1454–1460,

doi:10.1016/j.compositesa.2010.06.007.

12. Wagner, L.; Bader, T.K.; De Borst, K. Nanoindentation of Wood Cell Walls: Effects of Sample Preparation and Indentation Protocol. *J. Mater. Sci.* **2014**, *49*, 94–102, doi:10.1007/s10853-013-7680-3.
13. Li, J.; Yu, Y.; Feng, C.; Wang, H. Mechanical Characterization of Pinus Massoniana Cell Walls Infected by Blue-Stain Fungi Using in Situ Nanoindentation. *J. For. Res.* **2020**, *31*, 661–665, doi:10.1007/s11676-018-0848-6.
14. Vincent, M.; Tong, Q.; Terziev, N.; Daniel, G.; Bustos, C.; Escobar, W.G.; Duchesne, I. A Comparison of Nanoindentation Cell Wall Hardness and Brinell Wood Hardness in Jack Pine (Pinus Banksiana Lamb.). *Wood Sci. Technol.* **2014**, *48*, 7–22, doi:10.1007/s00226-013-0580-5.
15. Jakes, J.E.; Stone, D.S. Best Practices for Quasistatic Berkovich Nanoindentation of Wood Cell Walls. *Forests* **2021**, *12*, 1–41, doi:10.3390/f12121696.
16. Oliver, W.; Pharr, G. An Improved Technique for Determining Hardness and Elastic Modulus Using Load and Displacement Sensing Indentation Experiments. *J. Mater. Res.* 1992, *7*, 1564–1583.
17. Schuh, C.A. Nanoindentation Studies of Materials. *Mater. Today* **2006**, *9*, 32–40, doi:10.1016/S1369-7021(06)71495-X.
18. Hayes, S.A.; Goruppa, A.A.; Jones, F.R. Dynamic Nanoindentation as a Tool for the Examination of Polymeric Materials. *J. Mater. Res.* **2004**, *19*, 3298–3306, doi:10.1557/JMR.2004.0437.
19. Jakes, J.E.; Lakes, R.S.; Stone, D.S. Broadband Nanoindentation of Glassy Polymers: Part I. Viscoelasticity. *J. Mater. Res.* **2012**, *27*, 463–474, doi:10.1557/jmr.2011.363.
20. Jakes, J.E.; Lakes, R.S.; Stone, D.S. Broadband Nanoindentation of Glassy Polymers: Part II. Viscoplasticity. *J. Mater. Res.* **2012**, *27*, 475–484, doi:10.1557/jmr.2011.364.
21. Nayar, V.T.; Weiland, J.D.; Nelson, C.S.; Hodge, A.M. Elastic and Viscoelastic Characterization of Agar. *J. Mech. Behav. Biomed. Mater.* **2012**, *7*, 60–68, doi:10.1016/j.jmbbm.2011.05.027.
22. Placet, V.; Passard, J.; Perré, P. Viscoelastic Properties of Green Wood across the Grain Measured by Harmonic Tests in the Range 0-95°C: Hardwood vs. Softwood and Normal Wood vs. Reaction Wood. *Holzforschung* **2007**, *61*, 548–557, doi:10.1515/HF.2007.093.
23. Łukomski, M.; Bridarolli, A.; Fujisawa, N. Nanoindentation of Historic and Artists' Paints. *Appl. Sci.* **2022**, *12*, doi:10.3390/app12031018.
24. Chakravartula, A.; Komvopoulos, K. Viscoelastic Properties of Polymer Surfaces Investigated by Nanoscale Dynamic Mechanical Analysis. *Appl. Phys. Lett.* **2006**, *88*, doi:10.1063/1.2189156.
25. Venugopal, G.; Veetil, J.C.; Raghavan, N.; Singh, V.; Kumar, A.; Mukkannan, A. Nano-Dynamic Mechanical and Thermal Responses of Single-Walled Carbon Nanotubes Reinforced Polymer Nanocomposite Thinfilms. *J. Alloys Compd.* **2016**, *688*, 454–459, doi:10.1016/j.jallcom.2016.07.209.
26. Liu, K.; Ostadhassan, M.; Bubach, B.; Dietrich, R.; Rasouli, V. Nano-Dynamic Mechanical Analysis (Nano-DMA) of Creep Behavior of Shales: Bakken Case Study. *J. Mater. Sci.* **2018**, *53*, 4417–4432, doi:10.1007/s10853-017-1821-z.
27. Mallikarjunachari, G.; Ghosh, P. Pile-up Response of Polymer Thin Films to Static and Dynamic Loading. *Thin Solid Films* **2019**, *677*, 1–12, doi:10.1016/j.tsf.2019.01.040.
28. Panchal, V.; Dobryden, I.; Hangen, U.D.; Simatos, D.; Spalek, L.J.; Jacobs, I.E.; Schweicher, G.; Claesson, P.M.; Venkateshvaran, D. Mechanical Properties of Organic Electronic Polymers on the Nanoscale. *Adv. Electron. Mater.* **2022**, *8*, doi:10.1002/aelm.202101019.
29. Zhang, T.; Bai, S.L.; Zhang, Y.F.; Thibaut, B. Viscoelastic Properties of Wood Materials Characterized by Nanoindentation Experiments. *Wood Sci. Technol.* **2012**, *46*, 1003–1016, doi:10.1007/s00226-011-0458-3.

30. Wang, X.; Zhao, L.; Xu, B.; Li, Y.; Wang, S.; Deng, Y. Effects of Accelerated Aging Treatment on the Microstructure and Mechanics of Wood-Resin Interphase. *Holzforschung* **2017**, *72*, 235–241, doi:10.1515/hf-2017-0068.
31. Prošek, Z.; Králík, V.; Topic, J.; Nežerka, V.; Indrová, K.; Tesárek, P. A Description of the Microstructure and the Micromechanical Properties of Spruce Wood. *Acta Polytech.* **2015**, *55*, 39–49, doi:10.14311/AP.2015.55.0039.
32. Prošek, Z.; Topič, J.; Tesárek, P.; Nežerka, V.; Králik, V. Modulus Mapping and Its Use to Determine the Effect Process of Drying on the Cells of Spruce. *Key Eng. Mater.* **2016**, *714*, 25–28, doi:10.4028/www.scientific.net/KEM.714.25.
33. Wang, X.; Chen, X.; Xie, X.; Yuan, Z.; Cai, S.; Li, Y. Effect of Phenol Formaldehyde Resin Penetration on the Quasi-Static and Dynamic Mechanics Ofwood Cellwalls Using Nanoindentation. *Nanomaterials* **2019**, *9*, doi:10.3390/nano9101409.
34. Qin, L.; Lin, L.; Fu, F.; Fan, M. Micromechanical Properties of Wood Cell Wall and Interface Compound Middle Lamella Using Quasi-Static Nanoindentation and Dynamic Modulus Mapping. *J. Mater. Sci.* **2018**, *53*, 549–558, doi:10.1007/s10853-017-1185-4.
35. Li, Y.; Yin, L.; Huang, C.; Meng, Y.; Fu, F.; Wang, S.; Wu, Q. Quasi-Static and Dynamic Nanoindentation to Determine the Influence of Thermal Treatment on the Mechanical Properties of Bamboo Cell Walls. *Holzforschung* **2015**, *69*, 909–914, doi:10.1515/hf-2014-0112.
36. Lakes, R. *Viscoelastic Materials*; Cambridge University Press, New York: New York, 2009;
37. Jakes, J.E. Mechanism for Diffusion through Secondary Cell Walls in Lignocellulosic Biomass. *J. Phys. Chem. B* **2019**, *123*, 4333–4339, doi:10.1021/acs.jpcb.9b01430.
38. CONAF Plantaciones Forestales Available online: https://www.conaf.cl/nuestros-bosques/plantaciones-forestales/.
39. D2395, A. American Society for Testing Materials - ASTM D2395:14: Standard Test Method for Density and Specific Gravity (Relative Density) of Wood and Wood-Based Materials. *Annu. B. ASTM Stand.* **2014**, *93*, 1–13, doi:10.1520/D2395-14.2.
40. Meng, Y.; Wang, S.; Cai, Z.; Young, T.M.; Du, G.; Li, Y. A Novel Sample Preparation Method to Avoid Influence of Embedding Medium during Nano-Indentation. *Appl. Phys. A Mater. Sci. Process.* **2012**, *110*, 361–369, doi:10.1007/s00339-012-7123-z.
41. Jakes, J.E.; Frihart, C.R.; Beecher, J.F.; Moon, R.J.; Stone, D.S. Experimental Method to Account for Structural Compliance in Nanoindentation Measurements. *J. Mater. Res.* **2008**, *23*, 1113–1127, doi:10.1557/jmr.2008.0131.
42. Jakes, J.E. Improved Methods for Nanoindentation Berkovich Probe Calibrations Using Fused Silica. *J. Mater. Sci.* **2018**, *53*, 4814–4827, doi:10.1007/s10853-017-1922-8.
43. Stone, D.S.; Yoder, K.B.; Sproul, W.D. Hardness and Elastic Modulus of TiN Based on Continuous Indentation Technique and New Correlation. *J. Vac. Sci. Technol. A Vacuum, Surfaces, Film.* **1991**, *9*, 2543–2547, doi:10.1116/1.577270.
44. Asif, S.A.S.; Pethica, J.B. Nano-Scale Viscoelastic Properties of Polymer Materials. *Mater. Res. Soc. Symp. - Proc.* **1997**, *505*, 103–108, doi:10.1557/proc-505-103.
45. Syed Asif, S.A.; Pethica, J.B. Nanoindentation Creep of Single-Crystal Tungsten and Gallium Arsenide. *Philos. Mag. A Phys. Condens. Matter, Struct. Defects Mech. Prop.* **1997**, *76*, 1105–1118, doi:10.1080/01418619708214217.
46. Jakes, J.E.; Frihart, C.R.; Beecher, J.F.; Moon, R.J.; Resto, P.J.; Melgarejo, Z.H.; Suárez, O.M.; Baumgart,

H.; Elmustafa, A.A.; Stone, D.S. Nanoindentation near the Edge. *J. Mater. Res.* **2009**, *24*, 1016–1031, doi:10.1557/jmr.2009.0076.

47. Baradit, E.; Fuentealba, C.; Yáñez, M. Elastic Constants of Chilean Pinus Radiata Using Ultrasonic. *Maderas Cienc. y Tecnol.* **2021**, *23*, 1–10, doi:10.4067/S0718-221X2021000100427.
48. Herbert, E.G.; Oliver, W.C.; Pharr, G.M. Nanoindentation and the Dynamic Characterization of Viscoelastic Solids. *J. Phys. D. Appl. Phys.* **2008**, *41*, doi:10.1088/0022-3727/41/7/074021.
49. Jäger, A.; Bader, T.; Hofstetter, K.; Eberhardsteiner, J. The Relation between Indentation Modulus, Microfibril Angle, and Elastic Properties of Wood Cell Walls. *Compos. Part A Appl. Sci. Manuf.* **2011**, *42*, 677–685, doi:10.1016/j.compositesa.2011.02.007.
50. Liu, M.; Lyu, S.; Peng, L.; Fan, Z.; Cai, L.; Huang, Z.; Lyu, J. Study on Properties of Radiata Pine Wood Treated with Furfuryl Alcohol as Fretboard Materials for String Instruments. *Eur. J. Wood Wood Prod.* **2022**, *80*, 1185–1200, doi:10.1007/s00107-022-01829-z.
51. Erazo, O.; Moreno, P.; Valenzuela, P.; Gacitúa, W. Propriedades Nanomecânicas de Pinus Radiata D. Don Para Uso Em Produtos de Alto Valor / Nanomechanical Properties of Pinus Radiata D. Don for Use in High Value Products. *Brazilian J. Dev.* **2021**, *7*, 109892–109905, doi:10.34117/bjdv7n11-559.
52. Moon, R.J.; Jakes, J.E.; Beecher, J.F.; Frihart, C.R.; Stone, D.S. Relating Nanoindentation to Macroindentation of Wood. In Proceedings of the Advanced biomass science and technology for bio-based products, Beijing, China, 2009. Research Station; Hse, C., Jiang, Z., Kuo, M.L., Eds.; Chinese Academy of Forestry & USDA Forest Service, Southern Research Station, pp 145-160, 2009; pp. 145–160.
53. Wimmer, R.; Lucas, B. Comparing Mechanical Properties of Secondary Cell Wall and Cell Corner Middle Lamella in Spruce Wood. *IAWA J.* **1997**, *18*, 77–88.
54. Donaldson, L.A. S3 Lignin Concentration in Radiata Pine Tracheids. *Wood Sci. Technol.* **1987**, *21*, 227–234, doi:10.1007/BF00351394.
55. Gindl, W.; Gupta, H.S.; Grünwald, C. Lignification of Spruce Tracheid Secondary Cell Walls Related to Longitudinal Hardness and Modulus of Elasticity Using Nano-Indentation. *Can. J. Bot.* **2002**, *80*, 1029–1033, doi:10.1139/b02-091.
56. Jäger, A.; Hofstetter, K.; Buksnowitz, C.; Gindl-Altmutter, W.; Konnerth, J. Identification of Stiffness Tensor Components of Wood Cell Walls by Means of Nanoindentation. *Compos. Part A Appl. Sci. Manuf.* **2011**, *42*, 2101–2109, doi:10.1016/j.compositesa.2011.09.020.
57. Jiang, J.; Lu, J.; Yan, H. Dynamic Viscoelastic Properties of Wood Treated by Three Drying Methods Measured at High-Temperature Range. *Wood Fiber Sci.* **2008**, *40*, 72–79.
58. Jiang, J.; Lu, J. Impact of Temperature on the Linear Viscoelastic Region of Wood. *Can. J. For. Res.* **2009**, *39*, 2092–2099, doi:10.1139/X09-119.
59. Menard, K.P. *Dynamic Mechanical Analysis: A Pratical Introduction*; CRC Press, Boca Raton, FL, 1999; ISBN 0849386888.
60. Hay, J.; Herbert, E. Measuring the Complex Modulus of Polymers by Instrumented Indentation Testing. *Exp. Tech.* **2013**, *37*, 55–61, doi:10.1111/j.1747-1567.2011.00732.x.

 doi:10.20944/preprints202304.0708.v1